Intelligent-CCS Fed Marine-Express Model Train ME03 in Mass-Reduced-Mode

Kinjiro Yoshida, Hiroshi Takami and Hazime Mihara
Department of Electrical and Electronic Systems Engineering,
Kyushu University
10-1 6-chome Hakozaki Higasi-ku, Fukuoka 812-8581   Japan

ABSTRACT - This paper presents a new high-performance intelligent controlled current-source (CCS) system which can compensate for modelling errors of armature resistance, leakage and magnetizing inductances and for space harmonic components of speed EMF's. A shuttle-motion simulation is presented in the *mass-reduced-mode* in which an equivalent vehicle weight is reduced, by 40kg, from 47kg to 7kg.

This study provides one of the most important key-technologies in driving practical linear synchronous motor (LSM) Maglev vehicle.

1. INTRODUCTION

In 1989, the Marine-Express (ME) project, of which the basic concept is an amphibious linear motor (LM) car able to run both on land and under the water, was initiated at Kyushu University. A theory of new combined levitation and propulsion for the ME is proposed by Yoshida, one of the authors [1][2]. For the first time in the world, the underwater linear induction motor car ME01 [3] and LSM model car ME02 [4] have succeed in running under the water in the water tank because LM cars had never before been operated underwater .

The third LSM model car ME03 is a 1/5-th scale land travelling model train (see Fig. 1). ME03 has been levitated at a standstill [5] and propelled in the *mass-reduced-mode* [6] by applying the new combined levitation and propulsion method. It was shown experimentally that the ME03 train with three vehicles could run following very well the demand patterns for shuttle ground-flight [7].

In a practical Maglev system to which long-stator LSM is applied, there are the following important differences as compared with rotating machines :

(1) Impedance drops due to armature resistance and leakage inductance are generally much larger.

(2) Carrier frequency of inverter is much lower due to its very large capacity and the use of GTO.

(3) A sampling time is much larger due to special position-and-speed-sensing system along the very long guideway.

In addition, armature resistance, leakage and magnetizing inductances deviate from their normal values due to the change of levitation height, temperature in armature windings, distortion of guideway, space-harmonic components of speed EMF's, and so on. Vehicle position and speed can not be measured with high accuracy for a very long distance. These errors lead to a bad influence on current control. The current-control errors due to all these causes are increased extensively. It is necessary to solve the problems in order to realize Maglev vehicle control [8].

Conventional CCS which is generally used in rotating machines can not be applied to this Maglev vehicle. Control of two freedoms including voltage-model has to be introduced to compensate for the causes of current-control error mentioned above. The voltage-model can be derived from the rotating-machine model with fictitious variation of rotor radius [9].

Especially in the ME03, a controlled current-source (CCS) with higher frequency-characteristics of more than 100kHz has been applied to verify experimentally the principle of combined levitation-and-propulsion Maglev vehicle. But much cheaper general-purpose high-power inverter is inevitably required for a practical use.
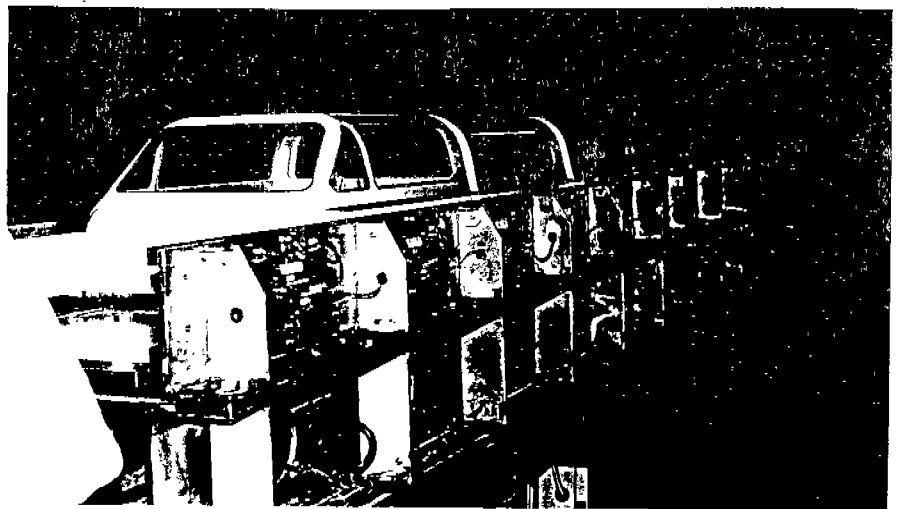

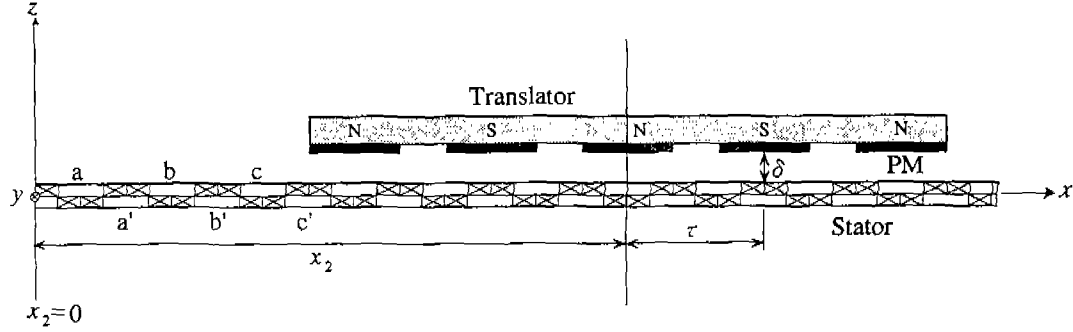Fig. 1   ME03 running on land and its LSM guideway.

Fig.2 Combined propulsion-and-levitation system in ME03.

This paper presents dynamics simulations of high-performance CCS applied to the ME03 running in the *mass-reduced-mode*. The CCS proposed here can compensate for the current-control errors by intelligent control of two freedoms on basis of *dq*-voltage model including space harmonics of the speed EMF's. It is operating with a relatively low frequency of 1kHz corresponding to sampling time of 1ms.

2. VOLTAGE MODEL FOR CCS ON THE DQ REFERENCE FRAME

Figure 2 shows the longitudinal cross-section of a long-stator LSM with a flat arrangement of PM's. The stator has only three-phase double-layer windings consisted of air-core coils. The translator is made of an array of PM's with alternating polarity fixed on a magnet yoke of steel or laminated iron. The end effect of PM LSM in Fig. 2 can be almost neglected, so that we can obtain an analytical-model expressed equivalently as a rotating machine with 2-pole PM as shown in Fig. 3. Variation of airgap-length δ due to levitation motion of the translator can be considered as fictitious variation of rotor radius in an equivalent rotating machine model (Fig. 3). Since many space-harmonic components are contained in the stator flux interlinkage, it is necessary to derive the voltage equations considering their influences.

Considering that δ varies instantaneously, a following equation is derived from the voltage equations [9].

$$v_s = r_s i + \left(L_s p + v_\delta \frac{\partial L_s}{\partial \delta} \right) i_s$$

$$+ \sum_{n=1} \left(v_{x2} D_{sn} \Psi_{fn} + v_\delta H_{sn} \frac{\partial \Psi_{fn}}{\partial \delta} \right) \tag{1}$$

where

$$H_{sn} = \begin{bmatrix} \cos n(\frac{\pi}{\tau} x_2 + \phi_n) \\ \cos n(\frac{\pi}{\tau} x_2 + \phi_n + \frac{4}{3}\pi) \\ \cos n(\frac{\pi}{\tau} x_2 + \phi_n + \frac{2}{3}\pi) \end{bmatrix}, \quad D_{sn} = \frac{\partial H_{sn}}{\partial x_2},$$
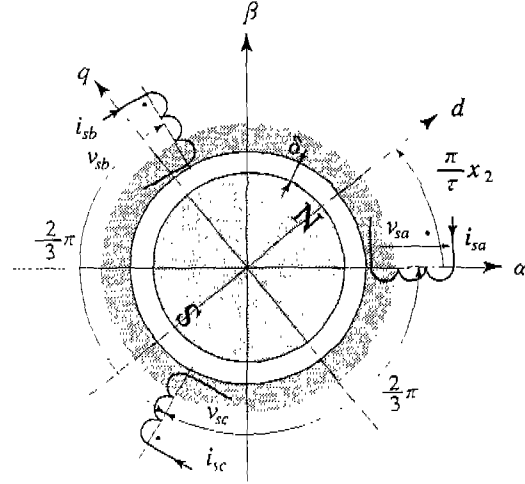

Fig.3 Rotating machine model for analysis.

and v_s, i_s are the armature phase-voltage and current, L_s the self-inductance represented by matrix forms, respectively. r_s is the armature resistance, Ψ_{fn} the nth order harmonic-component of armature flux-interlinkage by PM's and p = d/dt. x_2 is the vehicle position and v_{x2}, v_δ the vehicle speed in the propulsion and levitation directions, respectively.

The third and fifth terms are particular EMF's due to a levitation motion in Maglev system and have never been considered in conventional rotating machine theory.

Transforming into direct and quadrature axes d and q on the rotor reference frame revolving at synchronous speed,

$$v_s^{dq} = r_s i_s^{dq} + \left(\frac{\pi}{\tau} v_{x2} L_{sd}^{dq} + L_s^{dq} p + v_\delta \frac{\partial L_s^{dq}}{\partial \delta} \right) i_s^{dq} + \sum_{n=1,4,7,} v_{x2} D_{fn}^{dq} \Psi_{fn}^{dq}$$

$$+ \sum_{n=2,5,8} v_{x2} D_{hn}^{dq} \Psi_{fn}^{dq} + \sum_{n=3,6,9} v_{x2} D_{0n}^{dq} \Psi_{fn}^{dq} \tag{2}$$

where

$$L_s^{dq} = \begin{bmatrix} l_s & 0 & 0 \\ 0 & L_{sn} & 0 \\ 0 & 0 & L_{sn} \end{bmatrix}, \quad L_{sd}^{dq} = \begin{bmatrix} 0 & 0 & 0 \\ 0 & 0 & -L_{sn} \\ 0 & L_{sn} & 0 \end{bmatrix},$$

$$L_{sn} = l_s + (3/2)M_s, \quad \Psi_{fn}^{dq} = \sqrt{3/2}\Psi_{fn},$$

$$H_{fn}^{dq} = \begin{bmatrix} 0 & \cos\left\{(n-1)\frac{\pi}{\tau} x_2 + n\phi_n\right\} & \sin\left\{(n-1)\frac{\pi}{\tau} x_2 + n\phi_n\right\} \end{bmatrix}^T,$$

$$H_{hn}^{dq} = \left[0 \quad \cos\left\{(n+1)\frac{\pi}{\tau}x_2 + n\phi_n\right\} \quad -\sin\left\{(n+1)\frac{\pi}{\tau}x_2 + n\phi_n\right\} \right]^T,$$

$$H_{0n}^{dq} = \left[\sqrt{2}\cos n(\frac{\pi}{\tau}x_2 + \phi_n) \quad 0 \quad 0 \right]^T.$$

$$D_{in}^{dq} = \frac{\partial H_{in}^{dq}}{\partial x_2} \quad (i=f,\, b,\, 0)$$

and l_s, M_s are leakage and mutual inductances, respectively. Superscript T is the transpositional operator.

Table 1 and 2 shows the normal parameters and harmonic components of flux interlinkage of PM LSM measured under the condition that the airgap-length δ is constant (4mm), respectively[9].

3. VEHICLE CONTROL AND CCS CONTROL SYSTEM

Figure 4 shows the block diagram for simulations to evaluate the performance of CCS on the condition that the ME03 is propelled for shuttle motion in the *mass-reduced-mode*. Thrust and lift forces are controlled independently by a decoupled control strategy [7] and the vehicle is run following the demand patterns for shuttle running motion.

The armature current are supplied by CCS controller which is controlled by optimal feedback-control of two freedoms with the voltage model compensating for space-harmonic EMF's and considering the variations of LSM parameters due to variation of airgap-length.

The intelligent-CCS is carried out according to the following procedure :

(1) Calculation of demand voltage v_{s0} which is obtained from a formula based on voltage model of (2).

(2) Calculation of error voltage Δv_s which is determined by PI controller in order to minimize the error between command and actual currents.

Table 1 Normal paramerers of PM LSM.

Armature resistance	r_s	8.776 Ω
Self inductance	L_s	24.97 mH
Mutual inductance	M_s	10.89 mH
Leakage inductance	l_s	14.08 mH

Table 2 Harmonic components of flux interlinkage.

n	ψ_{fn}	ϕ_n
1	0.905065	-3.160261
2	0.011907	-0.324268
3	0.001531	-0.007942
4	0.000808	-0.293660
5	0.010260	-0.653557
6	0.000492	-0.473524
7	0.002703	-0.004003
8	0.000356	-0.196509
9	0.000276	0.173941
10	0.000436	-0.285599

(3) Calculation of command voltage v_s^* obtained by the sum of v_{s0} and Δv_s.

The gains of PI controller are determined by try-and-error method so as to minimize the control error of armature current. The LSM system is simulated using electromechanical dynamics equations of voltage and propulsion motion.

The voltage equations contain also the space harmonics of EMF's.

4. SIMULATED RESULTS

In Fig.4, all the control blocks including the motion control, decoupled control and current control are operated at a sampling time of 1 msec, which is feasible in a practical Digital-Signal-Processor control system. The ME03 LSM system is calculated at the sampling time of 0.1 ms in order to simulate accurately the dynamics in this system. The simulations are carried out with shuttle motion is in *the mass-*
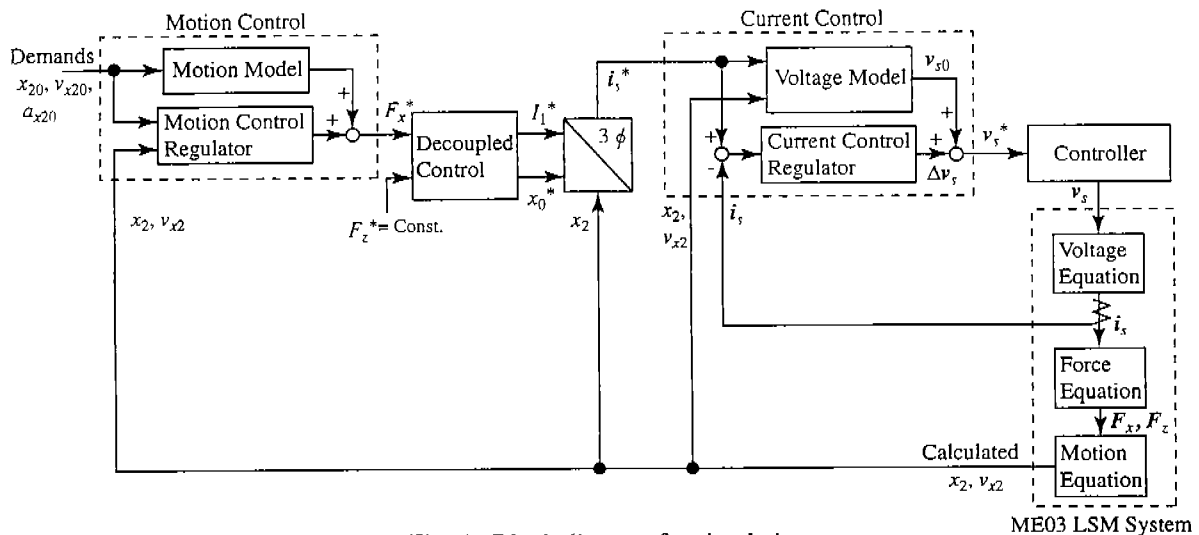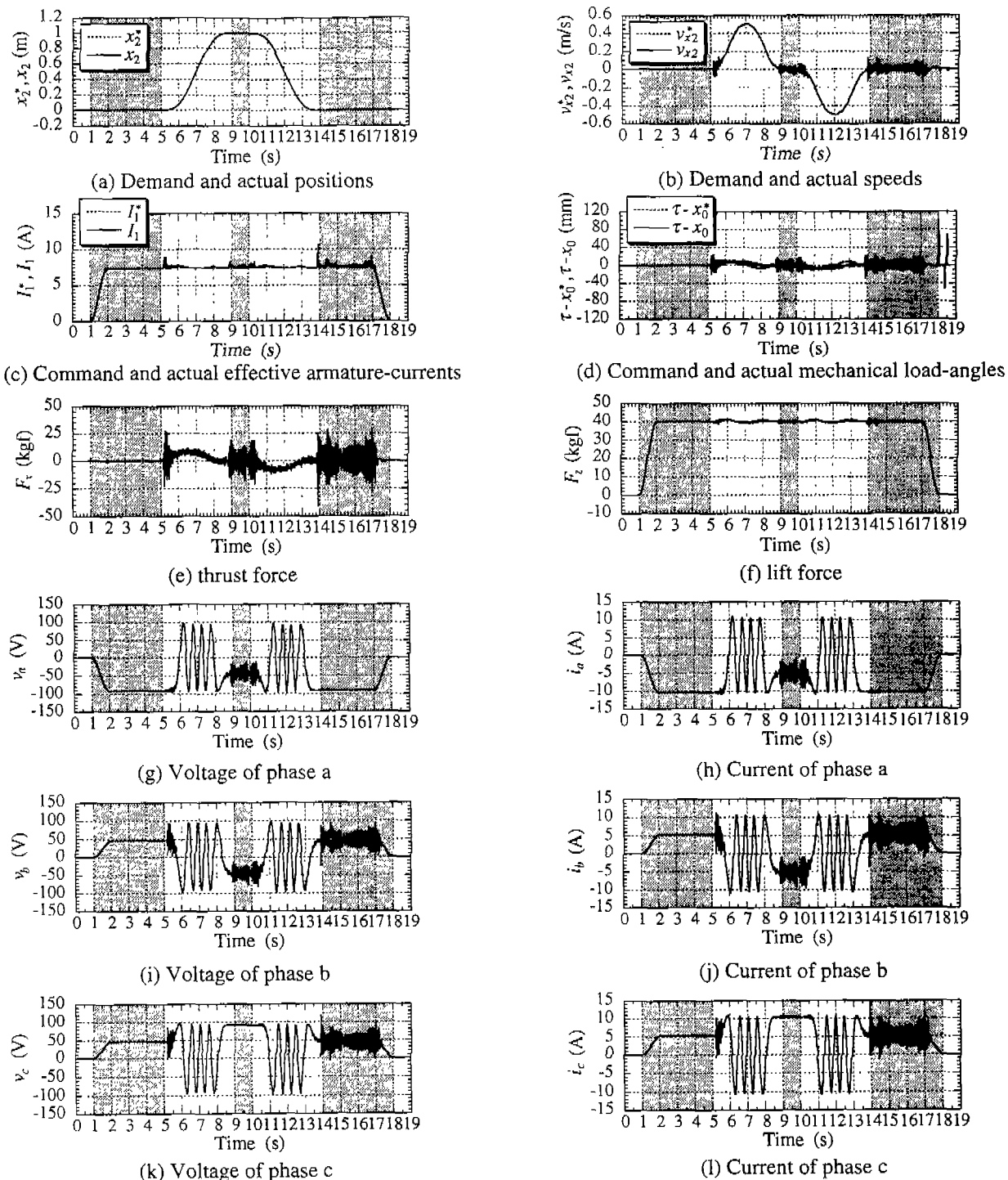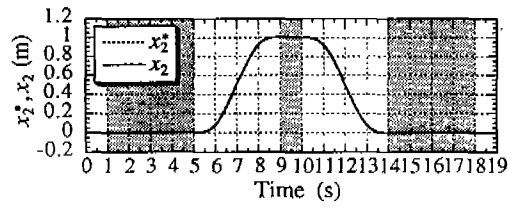

Fig. 4 Block diagram for simulations.

(a) Demand and actual positions
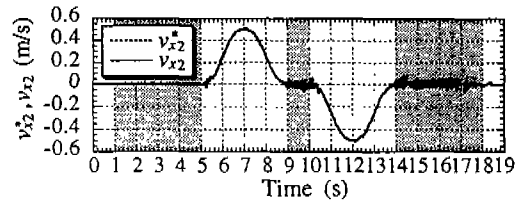
(b) Demand and actual speeds
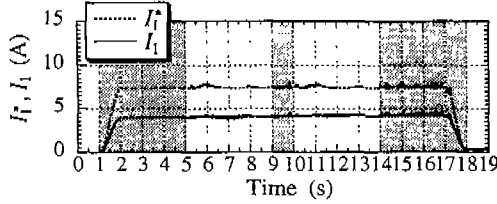
(c) Command and actual effective armature-currents

(d) Command and actual mechanical load-angles

(e) thrust force

(f) lift force

(g) Voltage of phase a

(h) Current of phase a

(i) Voltage of phase b

(j) Current of phase b

(k) Voltage of phase c

(l) Current of phase c

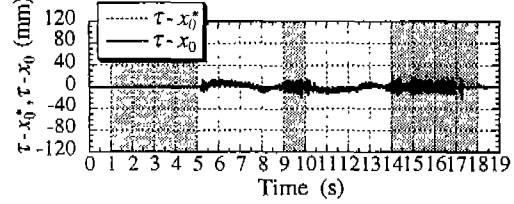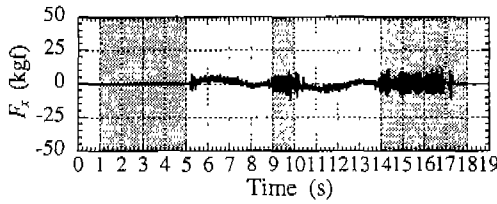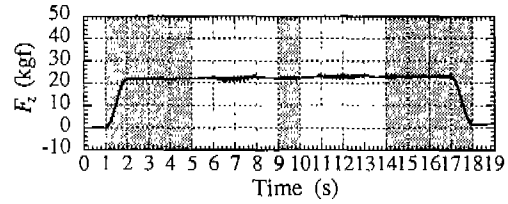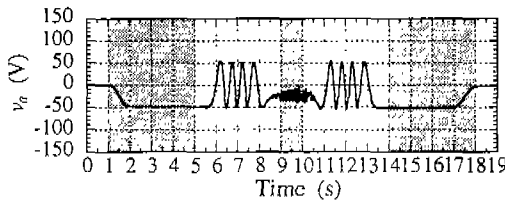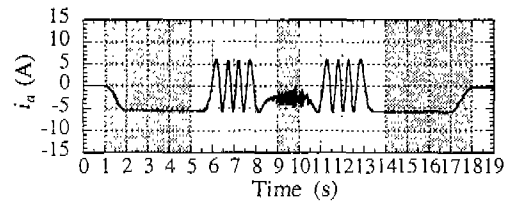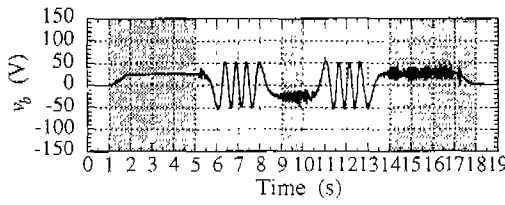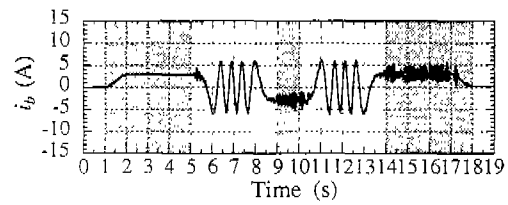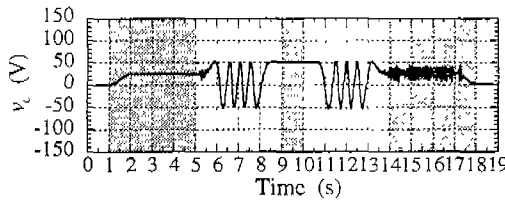Fig. 5 Dynamics simulation of ME03 fed CCS with voltage model (no modeling errors).

reduced-mode in which the vehicle weight on the supporting wheels is reduced by 40kg from 47kg to 7kg and air gap length δ is constant at 4mm.

Figure 5 shows the dynamics simulations of ME03 fed CCS with voltage model of which parameters correspond to those of LSM system. Figures 5 (a) and (b) show the vehicle position and speed, respectively. The solid line is the actual values and the dotted line is the demand values calculated from the motion equation of ME03 LSM system. Vehicle

position and speed follow the demand patterns very well and excellent trajectory control is achieved. Figures 5 (c) and (d) show the effective armature-current and complemental mechanical load-angle. Figures 5 (e) and (f) show the actual thrust and lift forces, respectively. In Fig.5 (f), the favorable control in the lift force is realized and this is due to the current control of two-freedom with voltage model proposed here. The ripples in the actual speed, mechanical load-angle and thrust force at the starting motion of 5.2sec

Fig. 6   Dynamics simulation of ME03 fed CCS with no voltage model.

and during the positioning phases of 9 to 10sec and 14 to 17.3sec are caused by the discrete position-and-speed sensors, nonlinear friction force and relatively large sampling time of 1ms. Figures 5 (g)-(l) are instantaneous voltage and current of each phase, respectively. The ripples in these figures are also caused by the same reasons in the above.

Figure 6 shows the dynamics simulations of ME03 fed CCS with no voltage model at the same condition in Fig.5. The ripples in Figs.6 (b), (d) and (e) are smaller than those

in Figs.5 (b), (d) and (e), but armature currents cannot only supply about 1/2-th the required current, like I_1 in Fig.6 (c) and i_a, i_b, i_c in Figs.6 (h), (j), (l). Accordingly the required lift-force cannot be obtained sufficiently in the *mass-reduced-mode* as shown in Fig.6 (f).

Figure 7 shows the control errors of armature currents in the CCS with voltage model as compared with CCS with no voltage model. The control errors in Fig.7 (a) are much less than Fig.7 (b). The control currents in CCS with voltage
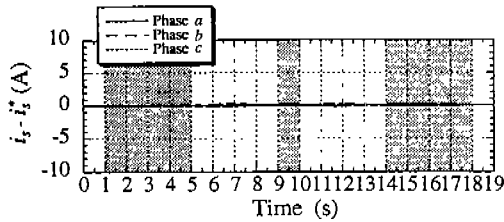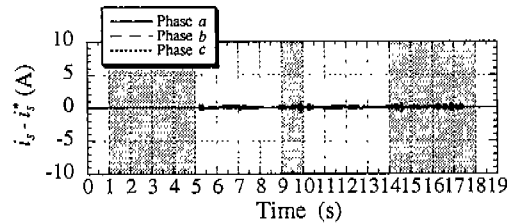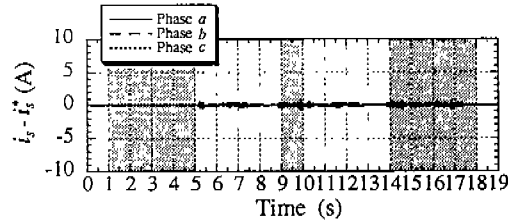
(a) CCS with voltage model
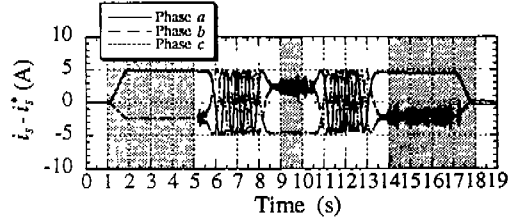
(b) CCS with no voltage model

Fig. 7 Control errors of armature currents in the CCS with and without voltage model(No modelling errors).

(a) CCS with voltage model (+20% resistance error)

(b) CCS with voltage model (+20% inductance error)

Fig. 8 Control errors of armature currents in the CCS with voltage model(modelling errors).

model follows very well their demand pattern.

Figures 8 (a) and (b) show current-control errors in the CCS with voltage model under the condition that the resistance and inductance are increased by 20% from the their normal values, respectively. It is confirmed that the proposed CCS is robust for variations of parameters and an excellent current-control including transient process can be achieved.

5. CONCLUSIONS

The proposed intelligent CCS control system has been successfully verified from simulations for shuttle motion at standstill and during acceleration and deceleration phases in the *mass-reduced-mode*. The *d-q* voltage-model derived from the rotating-machine model with fictitious variation of rotor radius. The CCS control system is an excellent current source which can automatically compensate for parameter errors of the *d-q* voltage model due to the change of temperature of armature windings, the distortion of guideway and space harmonics of the speed EMF's. In the CCS with no voltage-model, current-control errors is very large and the required lift force can not be obtained in the *mass-reduced-mode*.

This study of intelligent-CCS provides one of the most important key-technologies for practical Maglev vehicle.

REFERENCES

[1] K.Yoshida, "Linear Synchronous Motor Propulsion Method for Guided Vehicle,:"Japanese Patent Publication No. 1991-27703.

[2] K. Yoshida, H. Takami and L. Shi, "Decoupled-Control Method for Levitation and Propulsion in Amphibious Train Marine-Express,:"Memories of the Faculty of Engineering Kyushu University, vol.55, no.4, pp.467-489, Dec., 1995.

[3] K.Yoshida, H. Muta and N. Teshima, "Underwater Linear Motor Car,:"Journal of Applied Electromagnetics in Materials, vol.2, pp.275-280 , July, 1991.

[4] K. Yoshida, "Basic Study of Underwater Linear Motor Car ME02,:" Committee for the Studies Marine-Express Concept, ME Report No.3. 1991, Chap.1. pp.1-10.

[5] K. Yoshida, H. Takami, N. Shigemi and Y. Nagano, "Repulsive-Mode Levitation Control during a Standstill of a Land Travelling Marine-Express Model Train ME03," in Proc. of the 1994 ISEM-Seoul (book), pp.471-474.

[6] K. Yoshida, H. Takami,Y. Nagano and A. Sonoda, "Running Experiments of Marine-Express ME03 in Mass-Reduced-Control Mode," in 1995 National Convention Record I.E.E. Japan, No.1065.

[7] K. Yoshida, H. Takami,Y. Nagano and A. Sonoda, "A New Combined Levitation-and-Propulsion Control in Repulsive-Mode of a Land Travelling Marine-Express Model Train ME03," in Proc. of the 1996 ICEM, pp.242-247.

[8] M. Hashimoto, K. Kitano, K. Inden and H. Tanitsu, "Driving Control Characteristic Using the Inverter System at Yamanashi Maglev Test Line," in Proc. of the 1998 MAGLEV IEEJ, pp.287-291.

[9] K. Yoshida, H. Takami,T. Miyamoto and H. Mihara, "Position and Speed Observer in Marine-Express Model Train ME03 by EKF Compensating for Space-Harmonic EMF's," in Proc. of the 1998 PESC, pp.1854-1859.